Applied Physics B (2022) 128:59
https://doi.org/10.1007/s00340-022-07783-1

Applied Physics B
Lasers and Optics

On the assessment of de-noising algorithms in digital holographic interferometry and related approaches

Silvio Montrésor[1] · **Pascal Picart**[1,2]

Received: 20 December 2021 / Accepted: 13 February 2022 / Published online: 1 March 2022

Abstract
As a general rule, the development of specific processing algorithms requires to accurately simulate data of interest by generating it as close as possible to the reality. In digital holographic interferometry and related approaches, the experimental phase data that are used for metrology purposes are corrupted by the speckle decorrelation noise. Thus, they require to be processed with advanced algorithms. To check the performances of de-noising algorithms before applying to real experimental data, simulations have to be carried out to provide quantitative errors and other related metrics of those performances. In litterature, many published papers dealing with the problem of phase de-noising in digital holographic interferometry consider Gaussian statistics and the hypothesis of noise stationarity, for simulating test data. However, considering the point spread function of digital holographic imaging systems, the noise in the phase data does not follow the Gaussian statistics. This means that considering Gaussian noise in data simulations is to make a big mistake on the nature of the noise in the holographic system. Therefore, in this paper, one aims at demonstrating that the Gaussian statistics are not well appropriated for simulating noise in holography, because such an approach systematically overestimates the performances of the algorithms. Then, using appropriate metrics such as mean standard deviation error, quality index, and peak-signal-to-noise-ratio, the paper demonstrates that the realistic speckle noise must be taken into account and correctly simulated for benchmarking overall algorithm performances.

1 Introduction

Digital holography is an efficient method for metrology, both at the micro- and macro-scales [1]. Holographic phase imaging measures the optical path length related to the scene/object/structure of interest and the relevant data are wrapped modulo 2π phase that can be advantageously used for several purposes in basic research or industry: roughness measurements [2], surface shape profiling [3], surface deformation [4], or vibration measurements [5]. The method of holographic interferometry has the advantage of being contactless and non-intrusive by the use of light illumination but also provides full-field measurements. With the advent of very high-speed sensors, high temporal resolution can be obtained [5]. Thus, the approach is adapted to investigate fundamental properties of transient mechanical waves propagating in complex metamaterials [6]. The recent advent of long-wavelength infrared digital holography allows large deformation measurements, which are of interest for wide-field investigations [7]. In addition, such advances desensitize holographic measurement, since the wavelength is increased by a factor of almost 20 [4].

From the practical point of view, the change in the optical phase from digitally reconstructed holograms is of interest and is obtained modulo 2π. Basically, the speckle pattern produced from the object surface under coherent illumination is modified and changed from its initial state. It follows that the phase from holograms is also speckled. As a consequence, speckle decorrelation noise in included in phase changes, requiring advanced filtering to get noise-free phase maps [8, 9]. For that, a huge litterature related to the problem of de-noising in digital image processing is available. In addition to the de-noising problem, unwrapping of the modulo 2π phase is required to get a continuous phase map which is generally proportional to the measurand of the

✉ Pascal Picart
pascal.picart@univ-lemans.fr

[1] Laboratoire d'Acoustique de l'Université du Mans, CNRS 6613, Institut d'Acoustique-Graduate School (IA-GS), Le Mans Université, Avenue Olivier Messiaen, 72085 Le Mans, France

[2] École Nationale Supérieure d'Ingénieurs du Mans, rue Aristote, 72085 Le Mans Cedex 9, France

phenomenon under interest. Similarly as for de-noising, in litterature, a large diversity of unwrapping approaches can be found, each having its own specificities versus noise in phase maps, phase dislocations, or phase-fringe density.

For researchers and engineers, the development of specific processing algorithms requires to accurately simulate the phase data from digital holographic metrology. This point is a key point, because, as a geneal rule, performances of processing algorithms depend on the data used for the test of performances. The phase noise in data from holographic metrology and related approaches (shearography, speckle interferometry) is unconventional, since it has for figures of merit; first, the noise does not follow Gaussian statistics [10], second, the noise is amplitude-dependent (i.e., depends on the fringe density) [11], third, the noise is spatially correlated (its correlation length refers to the speckle grain size) [12], and fourth, the noise is anisotropic (i.e., depends on the sensor geometry) [13]. These have for consequences that the speckle noise in phase data is not stationary as can be the case for classical noises such as the photon noise, the electronic noise, or the quantization noise. It follows that realistic simulations of speckle phase noise to evaluate the performances of advanced processing algorithms have to consider the specificities of such a noise. However, without taking into account this physical reality, several papers related to the problem of phase de-noising in digital holographic interferometry did consider simulations with basic noise with Gaussian statistics with the hypothesis of stationarity [15–18]. In those papers, random Gaussian noise is added to the phase data to produce noisy modulo 2π phase maps. Therefore, this appears to be far from the reality, which is driven by light propagation and diffraction.

Therefore, this paper aims at demonstrating that the basic Gaussian noise is not well appropriated for simulating noise in holographic metrology, but that the realistic speckle noise must be taken into account according to the physics of the phenomenon. The paper is organized as follows: Sect. 2 presents the theoretical basics for realistic speckle noise simulations and Sect. 3 presents the methodology we followed for the demonstration. Section 4 presents the results of the comparison. Section 5 draws the conclusion of the study.

2 Basics of realistic noise simulations

2.1 Goal

The main objective of realistic simulations of speckle decorrelation noise is to yield phase maps including phase-fringe patterns corrupted with noise having rigorously the same properties as in real holographic systems. The simulated speckle noise must have the adequate probability density function (non-Gaussian) as well as correlation length corresponding to usual values for off-axis/on-axis digital holography. In addition, it has to be amplitude-dependent (dependent on the local fringe density) and according to the symmetry of the holographic system (possibly being anisotropic). At this point, for non-expert readers, we aim at giving few rapid explanations why the speckle noise does not follow Gaussian statistics and why it is dependent on the fringe density. We invite readers to consider papers [8, 11–13] which exhaustively describe the particular properties of the speckle decorrelation noise with experimental data supporting the theoretical analysis. The phase computed from digital holograms with an arctangent formulae is wrapped in the modulo 2π interval. This means it cannot exceed $+\pi$ or $-\pi$, so it statistically cannot reach infinite values. This has for consequence that, similarly, the decorrelation phase noise cannot exceed $+\pi$ or $-\pi$, and that it does not follow Gaussian statistics (that would reach values exceeding $+\pi$ or $-\pi$). Note that the probability density function of the phase noise is given in Eq. (4) in [12]. The decorrelation is amplitude-dependent, that is, it depends on the fringe density and fringe orientation. That was theoretically described in papers [11, 13]. In addition, in [13], experimental data perfectly fits theoretical data, thus clearly demonstrating this particular property of the speckle noise in holographic interferometry.

As a general rule, for simulations, a numerical model for the fringe pattern is required and can be chosen using classical mathematical functions such a Gaussian, polynoms, etc. This phase-fringe pattern corresponds to the phase change at the object surface between the two instants (or exposures). For example, this can be surface deformation due to vibration or heating. Generally, the surface deformation is related to the phase change by considering the observation and illumination conditions in the experimental set-up [1]. The simulation needs also to consider the roughness of the surface of the numerical object. From the surface roughness and deformation, two complex-valued fields can be computed, the first including the roughness, i.e., $A_1 = A_0 \exp(i\psi_0)$, and the last including both roughness and surface deformation, i.e., $A_2 = A_0 \exp(i\psi_0 + i\Delta\psi)$, $\Delta\psi$ being the phase change. Those two wavefronts are then propagated to the image plane through the digital holographic system. To get the phase change due to surface deformation and including the speckle noise decorrelation, the phase difference between the two propagated optical fields is calculated. According to the theoretical approaches for digital holography, and more generally for optical system, the holographic system can be considered as a filtering process between the initial object plane and the output image plane [1, 13, 14]. Therefore, the computation of the propagation of the two optical fields requires modelling for the point spread fonction (PSF) of the holographic system. This is discussed in the next subsection.

2.2 PSF of the digital holographic system

Whatever the optical configuration (Fresnel, Fourier, lensless Fourier, image-plane, microscopy) digital holographic imaging systems are linear system. Therefore, they can be approached using their PSF to describe the close relation between the initial object and the final digitally reconstructed image (complex-valued field). The basic relation between input and output optical fields through the linear holographic system is given by the convolution relation, according to Eq. (1) [1, 10, 12]

$$A_r(\mathbf{r}) = \mathrm{PSF}(\mathbf{r}) \otimes A(\mathbf{r}). \tag{1}$$

For the sake of compactness of the formulas, vector notation is adopted to designate the cartesian coordinates (x,y) of a point as $\mathbf{r}$. In Eq. (1), $\otimes$ means convolution, $A(\mathbf{r})$ is the input complex object field, and $A_r(\mathbf{r})$ is the image provided by the full holographic recording and processing. The PSF depends on the architecture. For example, for image-plane holography [12, 14] with pupil $p(\mathbf{r})$, wavelength λ, and focal length f, the *PSF* is given by Eq. (2) [10]

$$\mathrm{PSF}(x,y) = -\frac{i}{\lambda f}\exp\left(\frac{2i\pi f}{\lambda}\right)\exp\left(\frac{i\pi}{\lambda f}(x^2+y^2)\right) \times \int\int p(x',y')\exp\left(-\frac{2i\pi}{\lambda f}(x'x+y'x)\right)\mathrm{d}x'\mathrm{d}y'. \tag{2}$$

In this case, if the pupil is circular, then the PSF is isotropic and the noise also does. That means it does not depend on the fringe orientation. For the case of digital Fresnel holography [14], the PSF is given by Eq. (3) (ignoring the active surface of pixels):

$$\mathrm{PSF}(x,y) = MN\exp\left(-i\pi(N-1)\frac{xp_x}{\lambda d_0}\right)\exp\left(-i\pi(M-1)\frac{yp_y}{\lambda d_0}\right) \times \frac{\sin\left(\frac{\pi xNp_x}{\lambda d_0}\right)}{\sin\left(\frac{\pi xp_x}{\lambda d_0}\right)}\frac{\sin\left(\frac{\pi yMp_y}{\lambda d_0}\right)}{\sin\left(\frac{\pi yp_y}{\lambda d_0}\right)}, \tag{3}$$

with p_x, p_y the pixel pitch of the sensor, M, N the number of pixels and d_0 the distance between the sensor and the objet. If $M \neq N$ or $p_x \neq p_y$, then the *PSF* is anisotropic and the noise also does. That means it depends on the fringe orientation.

As a general rule, the *PSF* controls the speckle grain size in the reconstructed image plane. From a practical point of view, the convolution equation Eq. (1) can be computed with two-dimensional fast Fourier transforms.

The generation of phase noise in the phase difference can be approached from the point of view of spatial frequencies. In the pratical configurations, it can be considered that the holographic system described by its PSF, due to its limited spatial bandwidth, behaves as a low-pass filter and attenuates the high spatial frequencies corresponding to the strong slopes of the surface deformation. It follows that the speckle decorrelation noise is related to the modulation transfer function of the holographic imaging and that noise increases if the local slope of surface deformation increases [13]. Holographic imaging, as a linear filtering between the physical object and the digitally reconstructed image, disturbs the propagation of the spatial frequencies related to the deformation slope and this has for consequence the increase of the speckle decorrelation in the phase change. Consequently, the attenuation results in phase noise in the phase-fringe pattern between the two considered instants. Since strong surface deformation induces strong surface variations and thus strong deformation slopes and high fringe density, the noise is higher in regions where the fringe density is high and lower elsewhere.

2.3 Practical computation

For the practical computation to get realistic noisy phase maps, the convolution is realized through fast Fourier transform calculations. Equation (1) is expressed in the sens of Fourier transforms according to Eq. (4)

$$A_r = \mathrm{FT}^{-1}\left[\mathrm{FT}[A] \times P\tilde{S}F\right], \tag{4}$$

where FT means fast Fourier transform and $P\tilde{S}F$ is the Fourier transform of the PSF. Note that $P\tilde{S}F$ can be analytically known such as with Eq. (2,3) when considering their Fourier transforms [11, 13] or could also be numerically calculated using the equation of PSF (when known) and fast Fourier transform algorithm.

For setting the input optical fields A_i (i = 1,2), the roughness is numerically simulated by considering a random surface profile having Gaussian statistics and Dirac delta for autocorrelation function. This random surface generates a random optical phase ψ_0 uniformly distributed in the $[-\pi, +\pi$ [phase range [11]. The complex field at the surface, A_1, is calculated by considering a uniform amplitude for illumination. The complex field after the surface deformation, A_2, is computed by $A_2 = A_1\exp(i\Delta\psi)$. Then, the two images fields A_{r1} and A_{r2} are computed with Eq. (4). Finally, the individual phases are extracted and their phase difference yields the noisy phase $\Delta\psi_n$. The noise map is obtained by subtracting the noise phase to the theoretical noise-free map.

This way to simulate corrupted phase maps with speckle decorrelation noise is the only one to produce realisitic noise having the appropriate physical properties.

The next section discusses on the quantitative assessment of noise simulations by considering, on one hand, realistic noise simulations [11–13] and, on the other hand, classical Gaussian noise simulations [15–18].

3 Methodology

3.1 Databases

To get quantitative appraisal of the influence of the noise in the performances of processing algorithms, two databases were constitued. They were used to evaluate the perfomances of de-noising algorithms from litterature. The two databases include 25 phase-fringe patterns divided into 5 patterns and 5 different signal-to-noise ratios (SNR). The first database is obtained by adding stationary Gaussian noise, with the adequate SNR, to the noise-free phase data from the modelling. In that case, the level of noise is settled so as to get the same SNR as those obtained with speckle noise for each fringe pattern. Each pattern has its own noise realization. In the first database, the local SNR is not depending on the local fringe density. The second database is obtained by generating realistic speckle noise with non-Gaussian statistics and natural non-stationarity property, as discussed in Sect. 2. In the second database, the SNR depends on the fringe density and mimics realistic noise conditions, as those observed in experimental results [1, 12–14]. Note that for each fringe pattern, the SNR are almost equivalent in the two databases: the Gaussian noise is adjusted to yield the same SNR as given by the speckle simulator according to Eq. (5), by adjusting coefficient β

$$\Phi_{nG} = W[\Phi + \beta n], \tag{5}$$

with $W[\ldots]$ the wrapping operator, Φ the noise-free phase and n the Gaussian noise. Then, de-noising algorithms are applied to the two databases to de-noise the set of phase-fringe patterns. The phase errors are calculated using the noise-free reference phases. The ranking of the algorithms according to the phase errors may be generated by considering metrics.

3.2 Algorithms

The set of algorithms for the analysis was previously described in [12] and almost the same set is considered in [19–32]. As a brief reminder, the de-noising algorithms are: Gaussian filtering, median filtering, SAR filtering, Wiener filtering, wavelet thresholding approaches (such as Daubechies, symlets, curvelets, contourlets), non-local means filtering (NLMeans), anisotropic diffusion (Diffaniso) BM3D, and 2-D windowed Fourier transform filtering (Wtfr2). The reader is invited to consider [12] for the panel and details about the de-noising algorithms.

The set is completed with "Deep learning" algorithm that have been recently developed and applied to de-noise phase maps in digital holography [33–35], and with the dualtree wavelet transform [36], which has the advantage to yield good performances with very fast computational efficiency. A total of 39 selected de-noising algorithms were considered for the simulations. To keep clarity in figures, we have retained only the best 20 first methods considering each metric. Other else, for all simulations presented in the paper, the SNR are computed from the cosine image of the wrapped phase maps.

3.3 Metrics

The quantitative assessment requires choosing adapted metrics. The phase error (σ_ϕ) [12], the Q_{index} [37] and the peak-signal-to-noise ratio (PSNR) [38] were considered and are explicited in Eqs. (6, 7, 8) (Fig. 1):

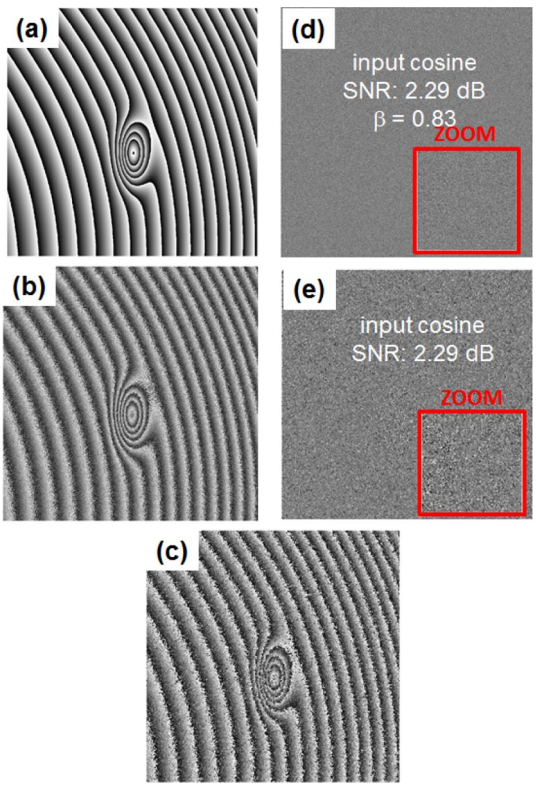

Fig. 1 Schemes of computation processes to generate noisy wrapped phase with speckle or Gaussian noise having same input cosine SNR; one can observe that in the case of speckle (zoom window), noise is dependent on the fringe density, thus being non-stationary: **a** noise-free phase, **b** phase map with added Gaussian noise, **c** phase map with generated speckle noise, **d** Gaussian noise map with zoom and input SNR for cosine with coefficient $\beta = 0.83$ to provide the same SNR as the speckle noise, and **e** speckle noise map with zoom and input SNR for cosine at 2.29 dB, similarly as the Gaussian SNR in **d**

$$\sigma_\phi = \sqrt{\frac{1}{MN}\sum_{i,j} r(i,j)^2 - \left(\frac{1}{MN}\sum_{i,j} r(i,j)\right)^2}, \tag{6}$$

$$Q_{\text{index}} = \frac{\sigma_{sd}}{\sigma_s \sigma_d}\frac{2\mu_s\mu_d}{\mu_s^2+\mu_d^2}\frac{2\sigma_s\sigma_d}{\sigma_s^2+\sigma_d^2}, \tag{7}$$

$$\text{PSNR} = 10\log 10\left(\frac{255^2}{\text{mse}}\right). \tag{8}$$

In Eq. (6), we have $r = \Delta\psi - \Delta\psi_d$, with $\Delta\psi$ being the known reference noise-free phase map and $\Delta\psi_d$ being the de-noised phase map. For the Q_{index} in Eq. (7), μ_s and μ_d are the mean values of $\Delta\psi$ and $\Delta\psi_d$, σ_s and σ_d are their variances and σ_{sd} their covariance. In Eq. (8), mse is the mean-squared error between the cosine of the reference noise-free phase map and the cosine of the de-noised phase map, both rescaled in the [0,255] interval.

4 Results

Figure 2 shows the rankings obtained for the two databases for the rms phase error. Figure 2a provides the ranking when considering the simulated Gaussian noise, whereas Fig. 2b provides the ranking for the realistic speckle noise. One observes that rankings obtained for both Gaussian and speckle noise are very similar. Particularly, rankings of the sixth first algorithms remain unchanged.

The best algorithm of the panel is the Wtfr2 [19], followed by Deep learning, dual tree wavelet transform, and curvelets. However, note that the rms phase error values are different: one observes variations of about 25% for the mean rms phase error. The rms phase error is underestimated when simulating Gaussian noise instead of using realistic speckle noise. The consequence is that the performances of all algorithms are overestimated.

Figure 3 provides the rms phase error versus the initial SNR in the phase images for 7 selected algorithms from the panel: deep learning, BM3D, anisotropic diffusion, symlet 8, dual tree wavelet transform, curvelets, and median 11×11. Figure 3a shows the rms phase error for the Gaussian noise and Fig. 3b that for the speckle noise. Both curves exhibit a "negative exponential" type shape. The decrease of the performance is not uniform over the range of the SNR in the database. Especially, one can note that the degradation of the performances (increase of the rms phase error) with simulated realistic speckle noise is more significant for low input SNR than for the Gaussian statistics. This means that when simulating noisy phase data using Gaussian statistics,

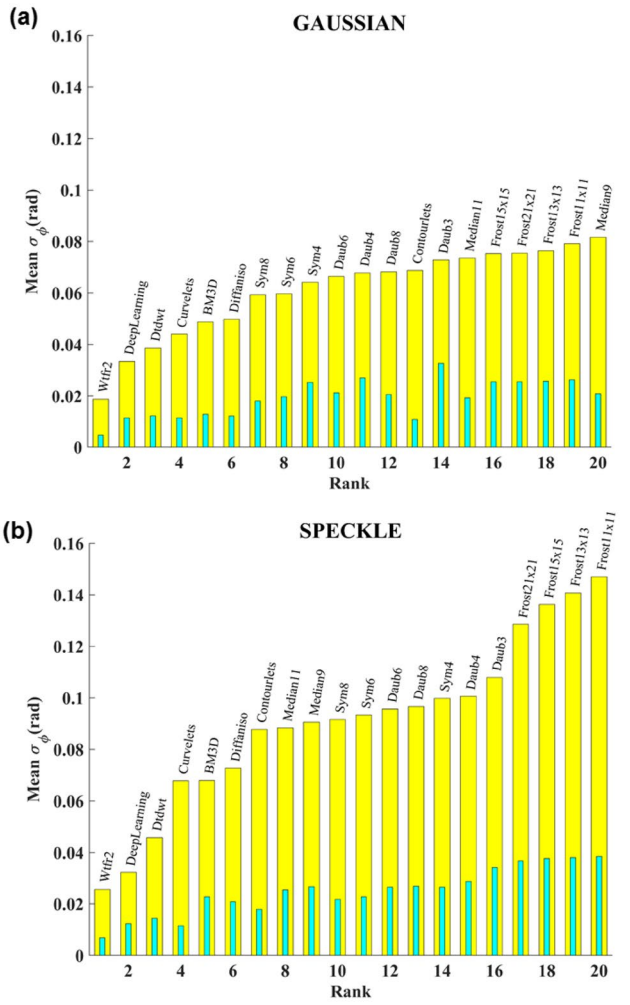

Fig. 2 Rankings of phase error for the 20 first de-noising algorithms: **a** Gaussian noise and **b** speckle noise

the performances are systemically overestimated, and even more for low SNR.

Note also that in Fig. 3b, stationary wavelets (sym8) and curvelets exhibit an increase of the rms phase error beyond 9 dB. Finally, observe that the Median 11×11 and sym8 algorithms both exhibit higher variances than other algorithms for both Gaussian and speckle cases.

Let us consider the Q_{index} metric: one can notice in Fig. 4 that rankings exhibit globally the same trends but that there do exist small differences. Therefore, if Wtfr2 appears first in both rankings, Dtdwt and Deep Learning do not appear in the same order in the overall ranking. Compared to the rms phase error, BM3D appears farther in both rankings, and stationary wavelets appear close to the top first places. However, one can see that in terms of values of the metric, algorithms are very close together from rank 4 to rank 15 whatever the considered noise statistics. These results are confirmed in Fig. 5 which exhibits very close trends for

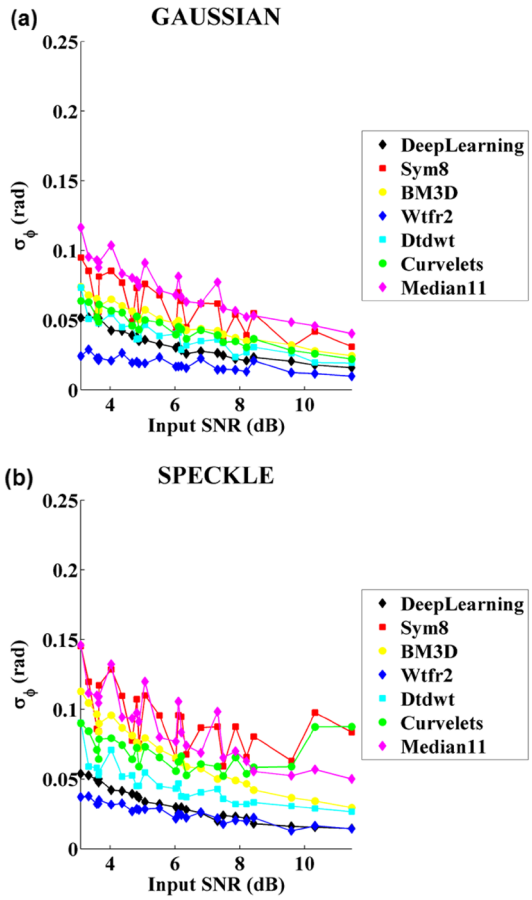

Fig. 3 Trends of 7 selected de-noising algorithms for phase error vs input cosine SNR: **a** Gaussian noise and **b** speckle noise

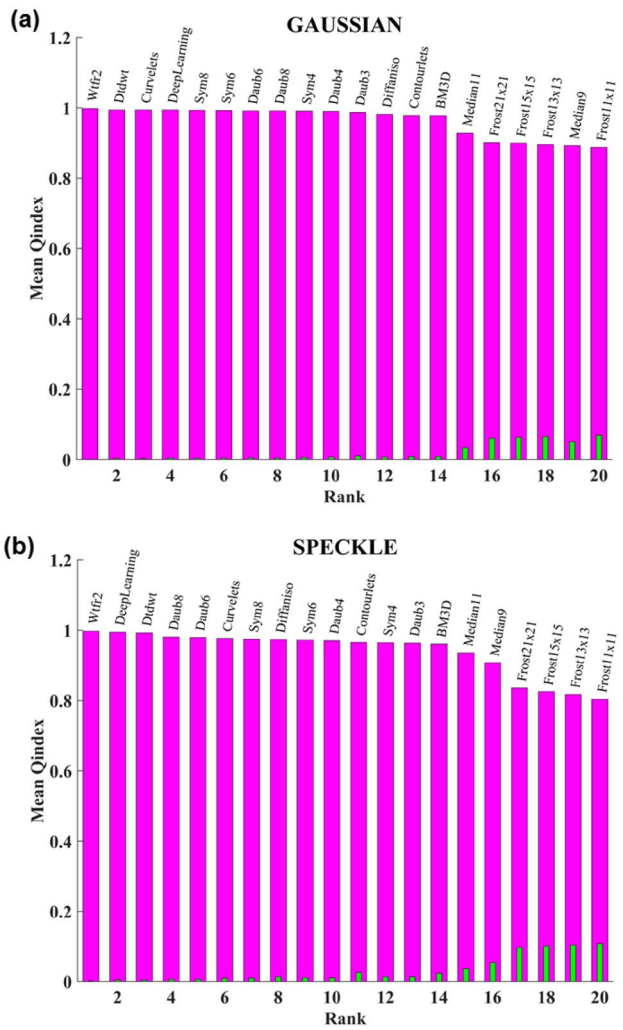

Fig. 4 Rankings of Q_{index} metric for 20 de-noising algorithms: **a** Gaussian noise and **b** speckle noise

the selected algorithms except BM3D and Median 11×11 for the Gaussian case. One observes with Sym8 that the decrease of performance in the case of speckle noise is about 9 dB. Considering Deep Learning, Wtfr2, Dtdwt, and BM3D algorithms, the metric are very close and constant in the range [8, 12] dB whatever the considered statistics.

In Fig. 6, rankings are obtained when considering the PSNR metric. In the six first ranks, the same algorithms are found with the same order except BM3D and curvelets which are permuted. In the rest of the rankings, one can clearly see that families of algorithms are grouped at the same place for both statistics. These are, respectively, stationary wavelets, Frost and NL_means algorithms. Overall, the PSNR metric is surrestimated of about 3 dB using Gaussian statistics rather than speckle ones, but there are strong differences between algorithms. For example, PSNR for BM3D is 36 dB with Gaussian noise and 32 dB with speckle noise. Considering Deep Learning, the PSNR exhibits almost the same values for both statistics, and there does exist small underestimation of 0.25 dB in case of the Gaussian noise. This is simply explained by the fact that Deep Learning is the only algorithm that has been trained specifically with speckle noise [33]. Considering Wtfr2, noticeable differences do exist between both statistics, and clearly, the PSNR is surrestimated of about 3 dB. In Fig. 7, the previous remarks are confirmed with trends, and one can clearly see that Deep learning exhibits same trends for both statistics for the whole range of input SNR. Except Deep learning, one can see that all methods among the seven selected exhibit a difference of about 2.5 dB for the PSNR between Gaussian and speckle cases.

In Figs. 8, 9 and 10, we display only differences of metric values versus input SNR, between the Gaussian case and the speckle case. For example, in Fig. 8a, each bar represents for a given method the average differences between the standard phase error computed in cases of Gaussian noise and speckle noise. In Fig. 8b, for a given

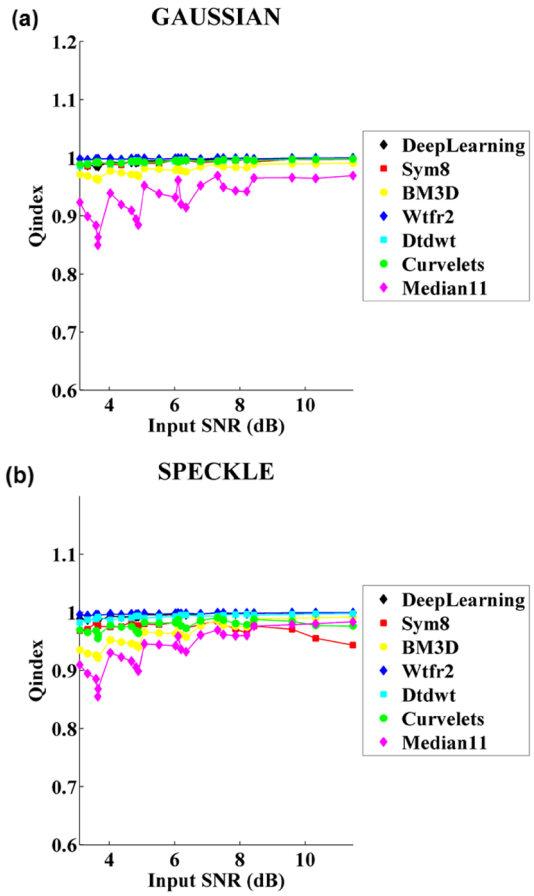

Fig. 5 Trends of 7 selected de-noising algorithms for phase error vs input cosine SNR: **a** Gaussian noise and **b** speckle noise

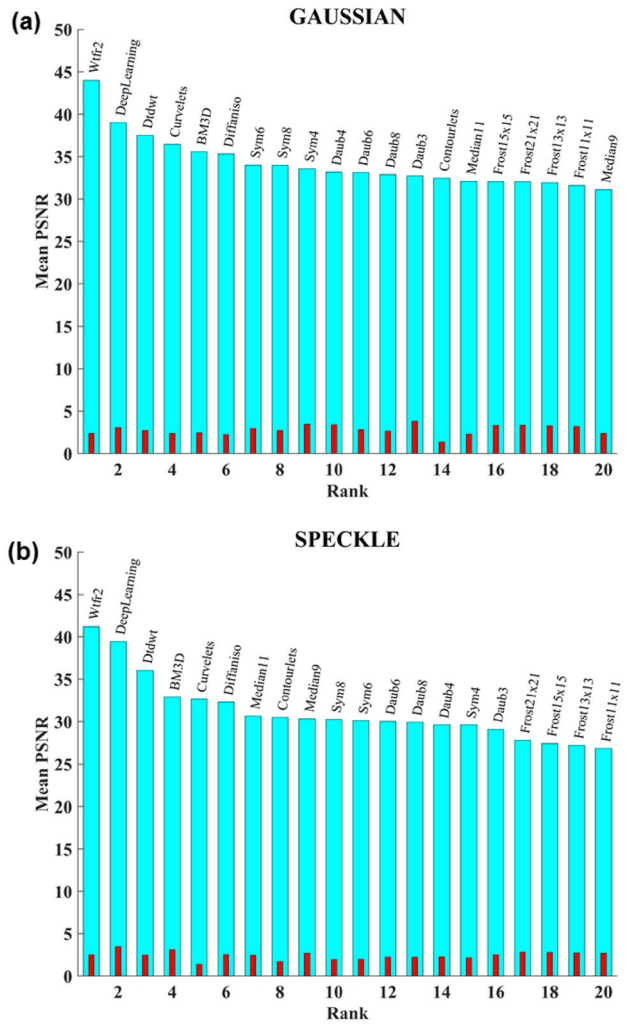

Fig. 6 Rankings of PSNR metric for 20 de-noising algorithms: **a** Gaussian noise and **b** speckle noise

selected method among the 7 displayed, the evolution of those differences versus the input SNR are plotted. Figures 8, 9 and 10 report, for each metric, values of the subtraction between statistics and for all algorithms. Then, those values were ranked. It appears in Fig. 8a that deep learning has a small underestimation in terms of phase error and that this trend remains constant over the input SNR range (see Fig. 8b). Median 5×5 exhibits the same results for both statistics and median 21×21 exhibits also small underestimation. In terms of Quality index, note in Fig. 9 that Dtdwt, Wtfr2, and deep learning algorithms are not sensitive nor to input SNR neither to statistics. In Fig. 9a, large median filters (kernel at 13, 15, or 21) are not impacted by the noise statistics. This is due to the fact that such methods have strong errors regarding the fringe structures, even more than the noise error itself. In Fig. 10, ranking of the differences of performances for Gaussian and speckle noise exhibits very close results than those given in Fig. 8. This is explained by the fact that phase error and cosine PSNR are closely linked by an algebraic approximation [38].

5 Conclusion

This paper discusses on the influence of the noise statistics from the point of view of the performances of de-noising algorithms in digital holographic interferometry and other related approaches in which the phase map is corrupted by speckle decorrelation noise. The discussion of the paper is related to the difference of performances when simulating noise in the phase data. On one hand, the simulations can be carried out according to the physical properties of the optical system by taking into account its point spread function. That does mimic the physical reality. On the other hand, basic noise simulation can be obtained by simply adding Gaussian

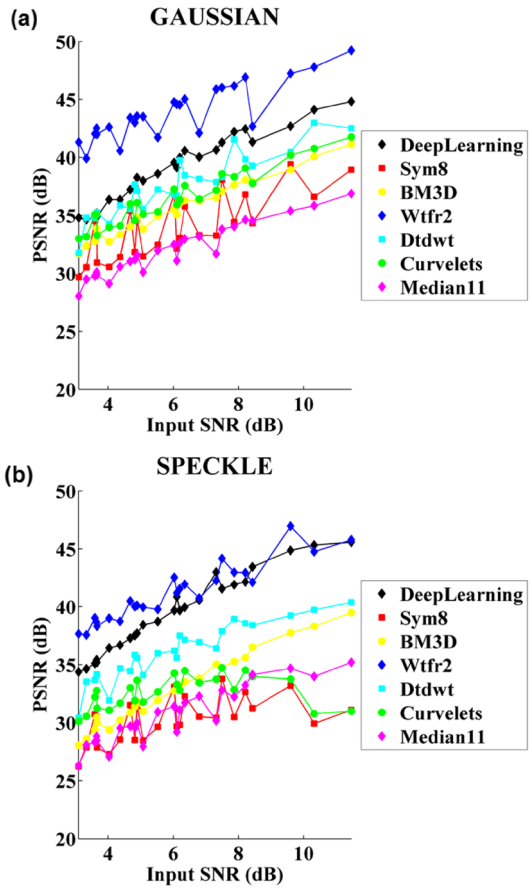

Fig. 7 Trends of 7 selected de-noising algorithms for PSNR vs input cosine SNR: **a** Gaussian noise and **b** speckle noise

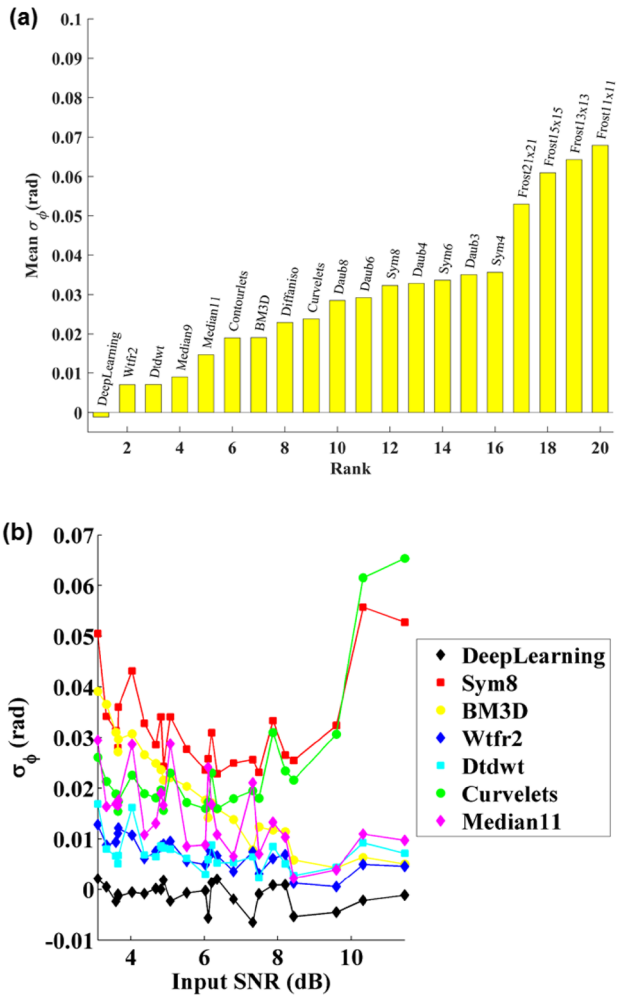

Fig. 8 Difference of performances for Gaussian noise and speckle noise for the phase error: **a** ranking of differences for the 20 algorithms; **b** trends of differences of phase error vs input cosine SNR for 7 selected algorithms

noise to the phase. That corresponds to what is usually proposed for simulating noise in images, from the general point of view. A set of 39 de-noising algorithms from literature were chosen and used to process two databases of phase-fringe patterns.

Gaussian and speckle statistics are considered for the comparison of the performances of the algorithms.

Results demonstrate that, although rankings are close together whatever the simulated statistics, the standard deviations of the phase errors are different for each algorithm. The performances obtained with the Gaussian statistics are systemically overestimated compared to those obtained with the speckle statistics. This means that if new algorithmic approaches are tested with noisy phases obtained with basic Gaussian simulations, then the evaluated performances will be better than that which would be obtained with real data. Thus, this may be a delicate issue for the real-life applications of the algorithm where the performances will fall short of expectations. As a conclusion, for more accurate simulations of algorithm perfomances in digital holographic interferometry and related methods, the speckle noise statistics (non-Gaussian, non-stationary, amplitude-dependent, possibly anisotropic) need to be considered.

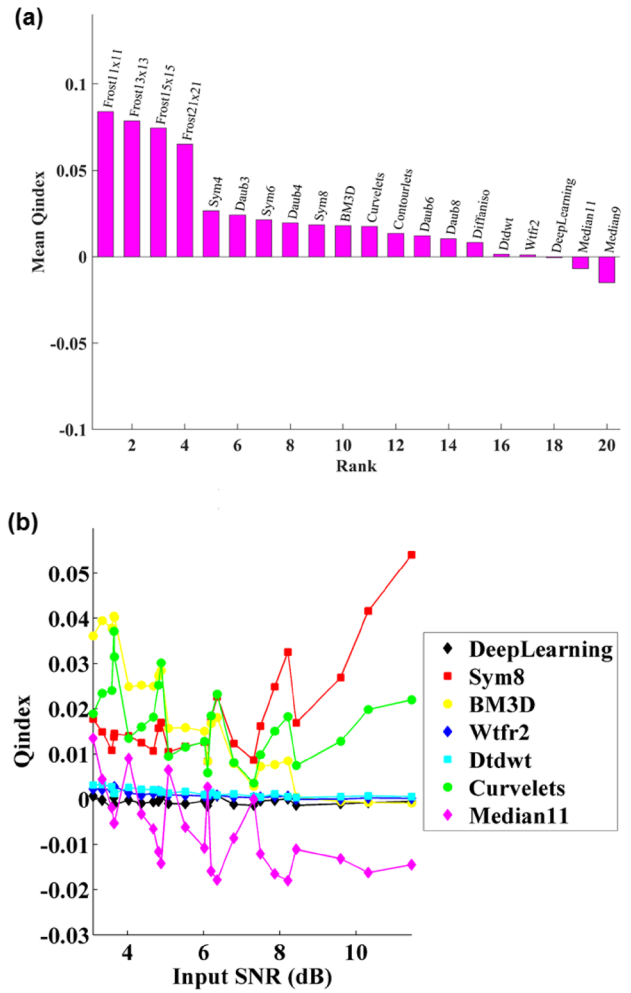

Fig. 9 Difference of performances for Gaussian noise and speckle noise for Q_{index} metric: **a** rankings of differences for the 20 algorithms; **b** trends of differences of Q_{index} vs input cosine SNR for 7 selected algorithms

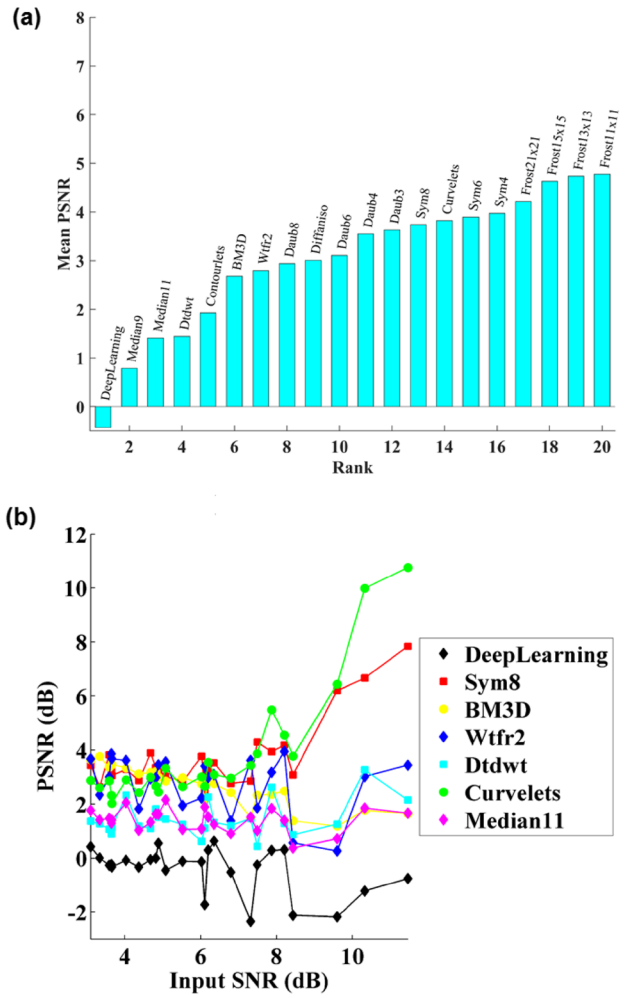

Fig. 10 Difference of performances for Gaussian noise and speckle noise for PSNR: **a** rankings of differences for the 20 algorithms; **b** trends of differences of PSNR vs input cosine SNR for 7 selected algorithms

References

1. P. Picart (ed.), *New Techniques in Digital Holography* (Wiley, New York, 2015)
2. T.M. Biewer, J.C. Sawyer, C.D. Smith, C.E. Thomas, Rev. Sci. Instrum. **89**, 10J123 (2018)
3. M. Fratz, T. Beckmann, J. Anders, A. Bertz, M. Bayer, T. Gießler, C. Nemeth, D. Carl, Appl. Opt. **58**, G120–G126 (2019)
4. M.P. Georges, J.-F. Vandenrijt, C. Thizy, Y. Stockman, P. Queeckers, F. Dubois, D. Doyle, Appl. Opt. **52**, A102–A116 (2013)
5. E. Meteyer, F. Foucart, M. Secail-Geraud, P. Picart, C. Pezerat, Mech. Syst. Signal Process. **164**, 108215 (2022)
6. L. Lagny, M. Secail-Geraud, J. Le Meur, S. Montresor, K. Heggarty, C. Pezerat, P. Picart, J. Sound Vib. **461**, 114925 (2019)
7. L. Valzania, Y. Zhao, L. Rong, D. Wang, M. Georges, E. Hack, P. Zolliker, Appl. Opt. **58**, G256–G275 (2019)
8. V. Bianco, P. Memmolo, M. Leo, S. Montresor, C. Distante, M. Paturzo, P. Picart, B. Javidi, P. Ferraro, Strategies for reducing speckle noise in digital holography. Light Sci. Appl. **7**, 48 (2018)
9. V. Bianco, P. Memmolo, M. Paturzo, A. Finizio, B. Javidi, P. Ferraro, Light. Sci. Appl. **5**, e16142 (2016)
10. J.W. Goodman, *Speckle Phenomena in Optics: Theory and Applications*, 2nd edn (SPIE, 2007)
11. M. Piniard, B. Sorrente, G. Hug, P. Picart, Theoretical analysis of surface-shape-induced decorrelation noise in multi-wavelength digital holography. Opt. Express **29**, 14720–14735 (2021)
12. S. Montresor, P. Picart, Quantitative appraisal for noise reduction in digital holographic phase imaging. Opt. Express **24**, 14322–14343 (2016)
13. E. Meteyer, F. Foucart, C. Pezerat, P. Picart, Modeling of speckle decorrelation in digital Fresnel holographic interferometry. Opt. Express **29**, 36180–36200 (2021)
14. M. Karray, P. Slangen, P. Picart, Comparison between digital Fresnel holography and digital image-plane holography: the role of the imaging aperture. Exp. Mech. **52**, 1275–1286 (2012)

15. K. Yan, Y. Yu, C. Huang, L. Sui, Q. Kemao, A. Asundi, Fringe pattern enoising based on deep learning. Opt. Commun. **437**, 148–152 (2019)
16. Z. Cheng, D. Liu, Y. Yang, T. Ling, X. Chen, L. Zhang, J. Bai, Y. Shen, L. Miao, W. Huang, Practical phase unwrapping of interferometric fringes based on unscented Kalman filter technique. Opt. Express **23**, 32337–32349 (2015)
17. J. Villa, J. Quiroga, I. De la Rosa, Regularized quadratic cost function for oriented fringe-pattern filtering. Opt. Lett. **34**, 1741–1743 (2009)
18. X. Chen, C. Tang, W. Xu, Y. Su, K. Su, General construction of transform-domain filters, filtering methods for electronic speckle pattern interferometry, and comparative analyses. Appl. Opt. **55**(9), 2214–2222 (2016)
19. Q. Kemao, Windowed Fourier transform for fringe pattern analysis. Appl. Opt. **43**, 2695–2702 (2004)
20. R.C. Gonzales, R.E. Woods, *Digital Image Processing*, 3rd edn. (Prentice Hall, Upper Saddle River, 2008)
21. V.S. Frost, J.A. Stiles, K.S. Shanmugan, J.C. Holtzman, A model for radar images and its application to adaptive digital filtering of multiplicative noise. IEEE Trans. Pattern Anal. Mach. Intell. PAMI **4**, 157–165 (1982)
22. J.S. Lee, Digital image enhancement and noise filtering by using local statistics. IEEE Trans. Pattern Anal. Mach. Intell. **2**, 165–1658 (1980)
23. P. Perona, J. Malik, Space scale and edge detection using anisotropic diffusion. IEEE Trans. Pattern Anal. Mach. Int. **12**(7), 629–639 (1990)
24. G. Gerig, O. Kubler, R. Kikinis, F.A. Jolesz, Nonlinear anisotropic filtering of MRI data. IEEE Trans. Med. Imaging **11**(2), 221–232 (1992)
25. S. Mallat, *A Wavelet Tour of Signal Processing* (Academic Press, New York, 1999)
26. D.L. Donoho, De-noising by soft-thresholding. IEEE Trans. Inf. Theory **41**, 613–627 (1995)
27. J.-L. Starck, E.J. Candès, D.L. Donoho, The curvelet transform for image denoising. IEEE Trans. Image Process. **11**, 670–684 (2002)
28. M.N. Do, M. Vetterli, The contourlet transform: an efficient directional multiresolution image representation. IEEE Trans. Image Proc. **14**(12), 2091–2106 (2005)
29. A. Buades, B. Coll, J. Morel, A non-local algorithm for image denoising. Proc. IEEE Comput. Soc. Conf. Comput. Vis. Pattern Recognit. **2**(2), 60–65 (2005)
30. A. Uzan, Y. Rivenson, A. Stern, Speckle denoising in digital holography by nonlocal means filtering. Appl. Opt. **52**(1), 195–200 (2013)
31. K. Dabov, A. Foi, V. Katkovnik, K. Egiazarian, Image denoising with block-matching and 3D filtering. In *Proceedings of SPIE 6064A-30* (2006)
32. P. Memmolo, M. Iannone, M. Ventre, P.A. Netti, A. Finizio, M. Paturzo, P. Ferraro, Quantitative phase maps denoising of long holographic sequences by using SPADEDH algorithm. Appl. Opt. **52**, 1453–1460 (2013)
33. S. Montresor, M. Tahon, A. Laurent, P. Picart, Computational de-noising based on deep learning for phase data in digital holographic interferometry. APL Photonics **5**, 030802 (2020)
34. S. Montresor, M. Tahon, A. Laurent, P. Picart, Deep learning speckle decorrelation de-noising for wide-field optical metrology. Proc. SPIE **11352**, 113520R (2020)
35. M. Tahon, S. Montresor, P. Picart, Towards reduced CNNs for de-noising phase images corrupted with speckle noise. Photonics **8**, 255 (2021)
36. I. Selesnick, R.G. Baraniuk, N.G. Kingsbury, The dual-tree complex wavelet transform. IEEE Signal Process. Mag. **22**(6), 123–151 (2005)
37. Z. Wang, A.C. Bovik, L. Lu, Why is image quality assessment so difficult? Proc. IEEE ICASSP **4**, 3313–3316 (2002)
38. S. Montrésor, P. Picart, M. Karray, Reference-free metric for quantitative noise appraisal in holographic phase measurements. J. Opt. Soc. Am. A **35**, A53–A60 (2018)